Model dielectric constants of GaP, GaAs, GaSb, InP, InAs, and InSb

Sadao Adachi
Electrical Communications Laboratories, Nippon Telegraph and Telephone Corporation, Atsugi-shi, Kanagawa 243-01, Japan
(Received 10 November 1986)

A new method is described for calculation of the real and imaginary parts of the dielectric function of semiconductors at energies below and above the lowest band gaps, in which the model is based on the Kramers-Kronig transformation and strongly connected with the electronic energy-band structures of the medium. This model reveals distinct structures at energies of the E_0, $E_0+\Delta_0$, E_1, $E_1+\Delta_1$, and E_2 critical points. Analyses are presented for GaP, GaAs, GaSb, InP, InAs, and InSb, and results are in satisfactory agreement with the experimental information over the entire range of energies. The model is able to properly give the optical constants, such as the refractive indices and the absorption coefficients, which are important for a variety of optoelectronic device applications.

I. INTRODUCTION

Studies of the optical properties of solids have proved to be a powerful tool in our understanding of the electronic structure of these solids. The dielectric function, $\epsilon(\omega)=\epsilon_1(\omega)+i\epsilon_2(\omega)$, is known to describe the optical properties of the medium at all photon energies $E=\hbar\omega$.[1] Real and imaginary parts of this dielectric function are connected by the Kramers-Kronig relations:

$$\epsilon_1(\omega)=1+\frac{2}{\pi}\int_0^\infty \frac{\omega'\epsilon_2(\omega')}{(\omega')^2-\omega^2}d\omega' , \tag{1a}$$

$$\epsilon_2(\omega)=-\frac{2}{\pi}\int_0^\infty \frac{\epsilon_1(\omega')}{(\omega')^2-\omega^2}d\omega' . \tag{1b}$$

Spectroscopic ellipsometry is an excellent technique to investigate the optical response of semiconductors and has been used to study Si,[2] Ge,[2,3] α-Sn,[4] most III-V semiconductors,[2,5–7] and CdSe.[8] On-line digitization of the data permits fast and efficient analysis of the structure observed in the $\epsilon(\omega)$ spectra in terms of standard analytic line shapes for interband critical points (CP's).[8] Numerical differentiation of the data facilitates this analysis.

Recently, Strössner *et al.*[9] have studied the refractive index of GaP and its pressure dependence. The data were fitted with a model dielectric constant which includes the lowest direct gap E_0, the corresponding bound exciton, and the E_1 gap as the dispersion mechanisms. Their model well explains the refractive-index dispersion at photon energies below the E_1 gap ($\sim$3.7 eV). However, the model does not take part in the dispersion above this energy, and the ϵ_2 spectrum predicted from this model is still far from the actual one.

In this paper, we present model dielectric constants, $\epsilon_1(\omega)$ and $\epsilon_2(\omega)$, which cover the optical response of semiconductors in the entire range of photon energies. In Sec. II, we describe the details of our model which includes the E_0, $E_0+\Delta_0$, E_1, $E_1+\Delta_1$, and E_2 gaps as the main dispersion mechanisms. We show in Sec. III the fits with our model to the experimental data for III-V compounds (GaP, GaAs, GaSb, InP, InAs, and InSb) reported previously. Dielectric-function-connected optical constants, such as the refractive indices and the absorption coefficients,[1] are easy to obtain from this study in the form of practical functions. Since the expressions obtained here are purely analytical functions of the fundamental electronic band parameters, the present model would also be applicable to the analysis of some perturbation-induced effects of the optical constants (e.g., the pressure and temperature dependence of the refractive index,[9] the piezobirefringence,[10] and light-scattering spectra[11,12]).

II. THEORETICAL MODEL

Optical properties of solids are known to be well explained by the optical joint density of states which becomes large for electronic transitions in the neighborhood of CP's. The critical points of some kind can occur as a consequence of the periodicity of the conduction- and valence-band energies in which case their position in **k** space is predictable from symmetry alone. Further critical points may also occur whose position cannot be predicted from symmetry.

The joint-density-of-states function $J_{cv}(\omega)$ can be related to the optical constant $\epsilon_2(\omega)$ as follows:

$$\epsilon_2(\omega)=\frac{4\hbar^2e^2}{\pi m^2\omega^2}|\langle c|p|v\rangle|^2 J_{cv}(\omega) , \tag{2}$$

where $\langle|p|\rangle$ is the momentum matrix element for v (valence)$\rightarrow c$ (conduction) transitions. In the following, we try to obtain the model dielectric functions for the CP's of various transition energies (E_0, $E_0+\Delta_0$, E_1, $E_1+\Delta_1$, and E_2). We also discuss the effects of indirect-gap transitions which will take an important part in the analysis of the ϵ_2 spectrum (Sec. III).

A. E_0 and $E_0+\Delta_0$ transitions

The lowest direct gaps in the zinc-blende-type semiconductors, such as GaP and InP, occur in the center of the Brillouin zone ($\mathbf{k}=0$), where it has fourfold (counting the two spin states) E_0 and twofold $E_0+\Delta_0$ gaps. First, we consider the contribution of the free electron-hole pair transitions to $\epsilon(\omega)$. The E_0 and $E_0+\Delta_0$ transitions are of the M_0 type. Assuming the bands are parabolic, the contribution to $\epsilon_2(\omega)$ of these transitions can be written as

$$\epsilon_2(\omega)=\begin{cases}\displaystyle\sum_{i=A,B,C}\frac{A}{3(\hbar\omega)^2}(\hbar\omega-E_{0i})^{0.5} & (\hbar\omega>E_0,\ \hbar\omega>E_0+\Delta_0)\ ,\\ 0 & (\hbar\omega<E_0)\ ,\end{cases} \tag{3}$$

with

$$A=\tfrac{4}{3}(\tfrac{3}{2}m^*)^{1.5}P^2\ . \tag{4}$$

In Eqs. (3) and (4), i stands for the E_0 ($\Gamma_8\rightarrow\Gamma_6;A,B$) and $E_0+\Delta_0$ gap transitions ($\Gamma_7\rightarrow\Gamma_6;C$), m^* is the combined density-of-states mass, and P^2 is the squared momentum matrix element. Substituting Eq. (3) into Eq. (1) and assuming P^2 independent of energy, we obtain[13,14]

$$\epsilon_1(\omega)-1=AE_0^{-1.5}\left[f(\chi_0)+\frac{1}{2}\left[\frac{E_0}{E_0+\Delta_0}\right]^{1.5}f(\chi_{0s})\right]\ , \tag{5}$$

with

$$f(\chi_0)=\chi_0^{-2}[2-(1+\chi_0)^{0.5}-(1-\chi_0)^{0.5}H(1-\chi_0)]\ , \tag{6a}$$

$$f(\chi_{0s})=\chi_{0s}^{-2}[2-(1+\chi_{0s})^{0.5}-(1-\chi_{0s})^{0.5}H(1-\chi_{0s})]\ , \tag{6b}$$

$$\chi_0=\hbar\omega/E_0\ , \tag{7a}$$

$$\chi_{0s}=\hbar\omega/(E_0+\Delta_0)\ , \tag{7b}$$

and

$$H(y)=\begin{cases}1 & \text{for } y\geq 0\ ,\\ 0 & \text{for } y<0\ .\end{cases} \tag{8}$$

Next, let us consider the contribution of the Wannier-exciton transitions to $\epsilon(\omega)$. The discrete series of exciton lines in the E_0 gap can be given by

$$\epsilon_2(\omega)=\frac{f^D}{(\hbar\omega)^2}\sum_{n=1}^{\infty}|\phi_n(0)|^2(E_{\rm ex}^n-\hbar\omega)\ , \tag{9}$$

with

$$|\phi_n(0)|^2=V_0/\pi a_0^{*3}n^3\ , \tag{10a}$$

$$E_{\rm ex}^n=E_0+\frac{\hbar^2K^2}{2M}-\frac{G}{n^2}\ . \tag{10b}$$

In Eqs. (9) and (10), f^D is the strength parameter, $\phi_n(0)$ the envelope function of the nth exciton state, V_0 the volume of the unit cell, a_0^* the exciton Bohr radius, K the exciton wave number, M the effective electron plus hole mass, and G is the exciton Rydberg energy. The Kramers-Kronig transformation of Eq. (9) gives[14]

$$\epsilon_1(\omega)-1=\sum_{n=1}^{\infty}\frac{F^D}{n^3[(E_{\rm ex}^n)^2-(\hbar\omega)^2]}\ , \tag{11}$$

with

$$F^D=2E_{\rm ex}^n n^3 f^D|\phi_n(0)|^2\pi^{-1}\ . \tag{12}$$

The continuum-exciton transitions have like free electron-hole pair characteristics, and the contribution of these transitions to $\epsilon(\omega)$ can be considered with expressions similar to Eqs. (3) and (5).[14]

The discrete-exciton term [Eq. (11)] gives a sharp dispersion compared with the continuum-exciton or the free electron-hole pair term [Eq. (5)]. However, the excitonic effect in materials of interest here is present at low temperatures only. The contribution of this effect is, thus, not important in the present analysis.

B. E_1 and $E_1+\Delta_1$ transitions

Band-structure calculations and some experimental work indicated[15] that the E_1 and $E_1+\Delta_1$ transitions take place along the $\langle 111\rangle$ directions (Λ) or at L points in the Brillouin zone. These CP's are of the M_1 type. The contributions to $\epsilon_2(\omega)$ of this type are

$$\epsilon_2(\omega)=\begin{cases}\pi\chi_1^{-2}[B_1-B_{11}(E_1-\hbar\omega)^{0.5}] & (\hbar\omega<E_1)\ ,\\ \pi B_1\chi_1^{-2} & (\hbar\omega>E_1)\end{cases} \tag{13a}$$

(13b)

for the E_1 transitions, and

$$\epsilon_2(\omega)=\begin{cases}\pi\chi_{1s}^{-2}[B_2-B_{21}(E_1+\Delta_1-\hbar\omega)^{0.5}] & (\hbar\omega<E_1+\Delta_1)\ ,\\ \pi B_2\chi_{1s}^{-2} & (\hbar\omega>E_1+\Delta_1)\end{cases} \tag{14a}$$

(14b)

for the $E_1+\Delta_1$ transitions, where

$$\chi_1=\hbar\omega/E_1\ , \tag{15a}$$

$$\chi_{1s}=\hbar\omega/(E_1+\Delta_1)\ . \tag{15b}$$

In Eqs. (13) and (14), B's are the strength parameters. Since the M_1 CP longitudinal effective mass is much larger than its transverse counterparts, one can treat these three-dimensional (3D) M_1 CP's as two-dimensional (2D) minima. The contribution to $\epsilon_2(\omega)$ of this type of 2D minima is given by

$$\epsilon_2(\omega)=\pi[B_1\chi_1^{-2}H(\chi_1-1)+B_2\chi_{1s}^{-2}H(\chi_{1s}-1)]\ , \tag{16}$$

where H's are functions defined by Eq. (8). The contribution of the E_1 and $E_1+\Delta_1$ transitions to $\epsilon_1(\omega)$ can be cal-

TABLE I. Parameters used in the calculation of $\epsilon_1(\omega)$ and $\epsilon_2(\omega)$.

Parameters	GaP	GaAs	GaSb	InP	InAs	InSb
E_0 (eV)	2.74	1.42	0.72	1.35	0.36	0.18
Δ_0 (eV)	0.10	0.34	0.74	0.10	0.40	0.81
E_1 (eV)	3.70	2.90	2.05	3.10	2.50	1.80
Δ_1 (eV)	<0.1	0.23	0.45	0.15	0.28	0.50
E_2 (eV)	5.0	4.75	4.0	4.7	4.45	3.9
E_g^{ID} (eV)	2.26 (X)	1.73 (L)	0.76 (L)	2.05 (L)	1.07 (L)	0.93 (L)
A	13.76	3.05	0.71	6.57	0.61	0.19
B_1	6.35	6.37	6.68	4.93	6.59	6.37
B_{11}	9.49	13.08	14.29	10.43	13.76	12.26
Γ (eV)	0.06	0.10	0.09	0.10	0.20	0.16
C	2.08	2.98	5.69	1.49	1.78	5.37
γ	0.132	0.168	0.290	0.094	0.108	0.318
D	4.6	24.2	7.4	60.4	20.8	19.5
$\epsilon_{1\infty}$	0.1	1.2	1.0	1.6	2.8	3.1

culated from Eq. (16) by using the Kramers-Kronig transformation. The result is

$$\epsilon_1(\omega)-1=-B_1\chi_1^{-2}\ln(1-\chi_1^2)-B_2\chi_{1s}^{-2}\ln(1-\chi_{1s}^2)\ . \tag{17}$$

The first and second terms in the right-hand side of Eq. (17) correspond to the E_1 and $E_1+\Delta_1$ gap contributions, respectively.

The dependence of ϵ_1 on frequency ω obtained from Eq. (17) is shown in Fig. 1. The numerical values used in the calculations correspond to those for GaAs (see Table I). The theoretical ϵ_1 spectrum exhibits a divergence at the E_1 CP energy. It is well known that the optical transitions are strongly affected by a damping effect, i.e., a lifetime broadening. The broadening parameter can be expressed by a sum of two different contributions: $\Gamma(T)=\Gamma_0+\Gamma_\Xi(T)$, where Γ_0 is independent of the temperature T, arising mainly from lattice defects, and $\Gamma_\Xi(T)$ is a contribution through emission and absorption of phonons of average frequency Ξ, proportional to $[\exp(\Xi/T)-1]^{-1}$.

The lifetime broadening effect can be easily introduced in Eq. (17) in a phenomenological manner by replacing ω by $\omega+i(\Gamma/\hbar)$.[11] Variation of $\epsilon_1(\omega)$ for a particular choice of the broadening energy Γ (0, 0.1, and 0.2 eV) is shown in Fig. 1 by the solid lines. As seen in the figure, the broadening effect can decrease the strength of the $E_1/E_1+\Delta_1$ structure and lead to a fact which is coincident with experimental verification.

As pointed out by Strössner *et al.*,[9] the parabolic bands extending to infinite energies implied by Eqs. (16) and (17) should be nonphysical. We, thus, modify the model by taking into account a cutoff at the energy E_c. This modification provides

$$\epsilon_2(\omega)=\pi[B_1\chi_1^{-2}H(\chi_1-1)+B_2\chi_{1s}^{-2}H(\chi_{1s}-1)]H(1-\chi_c) \tag{18}$$

and

$$\epsilon_1(\omega)-1=-B_1\chi_1^{-2}\ln\left[\frac{1-\chi_1^2}{1-\chi_c^2}\right]-B_2\chi_{1s}^{-2}\ln\left[\frac{1-\chi_{1s}^2}{1-\chi_c^2}\right], \tag{19}$$

with

$$\chi_c=\hbar\omega/E_c\ . \tag{20}$$

In Fig. 1, the dashed line represents the dependence of ϵ_1 on ω obtained from Eq. (19) ($E_c=6.0$ eV; $\Gamma=0.1$ eV). This cutoff correction lowers the E_1 and $E_1+\Delta_1$ gap contributions below E_c and gives a divergence close to this energy (see Fig. 5).

C. E_2 transitions

The more pronounced structure found in the higher-energy region than E_1 and $E_1+\Delta_1$ is usually labeled E_2. The nature of the E_2 transitions is more complicated

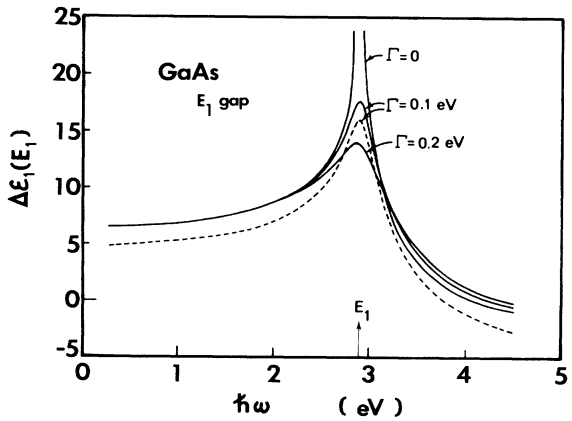

FIG. 1. Line shape of the E_1 gap contribution to $\epsilon_1(\omega)$ for GaAs [Eq. (18)] with three different damping parameters ($\Gamma=0$, 0.1, and 0.2 eV). The dashed line represents the dependence of ϵ_1 on ω with high-energy cutoff correction in Eq. (19) ($E_c=6.0$ eV, $\Gamma=0.1$ eV).

since it does not correspond to a single, well-defined CP.[3] Because of this fact, we shall characterize the E_2 structure as that of a damped harmonic oscillator:

$$\epsilon_2(\omega)=\frac{C\chi_2\gamma}{(1-\chi_2^2)^2+\chi_2^2\gamma^2}\ , \tag{21}$$

$$\epsilon_1(\omega)-1=\frac{C(1-\chi_2^2)}{(1-\chi_2^2)^2+\chi_2^2\gamma^2}\ , \tag{22}$$

with

$$\chi_2=\hbar\omega/E_2\ . \tag{23}$$

Here, the quantity C represents the strength of the interaction between the oscillator and the electromagnetic wave (photon) and γ is the damping factor. If γ is much smaller than 1, ϵ_2 then has a significant value only when χ_2 is close to 1.0.

D. Indirect-gap transitions

Transitions between states which are not vertical in an energy-band diagram are called indirect transitions. The transition mechanism at the indirect gap is known to be expressed by a second-order process in the perturbation. Using the result of second-order time-dependent perturbation calculation, we obtain the contribution of the indirect optical transitions to $\epsilon_2(\omega)$ as

$$\epsilon_2(\omega)=\begin{cases}\dfrac{D}{(\hbar\omega)^2}(\hbar\omega-E_g^{\rm ID}+\hbar\omega_q)^2 & (\hbar\omega>E_g^{\rm ID}-\hbar\omega_q)\ ,\\ 0 & (\hbar\omega<E_g^{\rm ID}-\hbar\omega_q)\ ,\end{cases} \tag{24}$$

where D is the indirect-transition strength parameter, $E_g^{\rm ID}$ the indirect-gap energy, and $\hbar\omega_q$ is the phonon energy taking part in the indirect transitions. In Eq. (24), only the phonon absorption process is taken into account. The phonon emission process remains possible, however, the only difference from the above case is the sign of the phonon energy. Unfortunately, there has been no expression for contribution to $\epsilon_1(\omega)$ of the indirect transitions. Analytical expressions for this contribution from the Kramers-Kronig transformation are also not yet available. In Sec. III, thus, we take into account the contribution of the indirect transitions only to $\epsilon_2(\omega)$ but not to $\epsilon_1(\omega)$.

Wemple and DiDomenico[16] have proposed a semiempirical single-effective-oscillator model to analyze refractive-index dispersion in more than 100 widely different solids and liquids. Their model requires two parameters, E_p and E_d, where the imaginary part of the dielectric constant (ϵ_2) of the material was assumed to be a δ function at energy E_p and the strength of an effective oscillator at energy E_p was defined to be $\pi E_d/2$.

Matters are complicated by the lack of agreement of the data, e.g., for GaAs, with the Wemple-DiDomenico model at the direct absorption edge. Afromowitz[17] has, therefore, proposed a modified model which takes into account the direct absorption edge (E_0). The ϵ_2 spectrum proposed by Afromowitz is an empirical one which agrees closely with the data on the low-energy side of the spectrum. The spectrum of his model is written as

$$\epsilon_2(\omega)=\begin{cases}\eta(\hbar\omega)^4 & (E_0\le\hbar\omega\le E_f)\ ,\\ 0 & \text{otherwise}\ ,\end{cases} \tag{25}$$

where

$$\eta=\pi E_d/2E_p^3(E_p^2-E_0^2)\ , \tag{26a}$$

$$E_f=(2E_p^2-E_0^2)^{0.5}\ . \tag{26b}$$

In Fig. 2, we compare our ϵ_2 spectrum with those of the Wemple-DiDomenico (arrow) and the Afromowitz model (dotted line). The dashed line is obtained from the sum of Eqs. (3), (16), [2D M_0], and (21). As we will see later, it shows a poor fit with experimental data in the spectrum region between the $E_0+\Delta_0$ and E_1 gap. In GaAs, a direct-gap material, the lowest conduction minimum is located at Γ and the second and third set of conduction minima, respectively, lay 0.31 eV (L) and 0.49 eV (X) above the Γ minimum. The lowest direct gap E_0 ($E_0+\Delta_0$) of GaAs, $\Gamma_8^v\rightarrow\Gamma_6^c$ ($\Gamma_7^v\rightarrow\Gamma_6^c$), is 1.42 eV (1.76 eV), and the indirect gaps E_g^L ($\Gamma_8^v\rightarrow L_6^c$) and E_g^X ($\Gamma_8^v\rightarrow X_6^c$) are, respectively, 1.73 and 1.91 eV at room temperature. The solid line is obtained from the sum of Eqs. (3), (13) [3D M_1], (21), and (24). A consideration of the indirect-gap contribution [E_g^L; Eq. (24)] can improve a fit to experimental data in the $E_0+\Delta_0$ and E_1 spectrum region. An important difference between the 2D minimum [E_0] and the 3D saddle point [M_1] is that the lower-energy side shoulder of the E_1 structure can be cut off in the M_0 CP while the shoulder is never cut off in the M_1 CP. A better fit to experimental data can be achieved using the M_1 CP model [Eq. (13)].

An individual contribution to ϵ_1 of the E_0, $E_0+\Delta_0$, E_1, and E_2 gaps for GaAs is shown in Fig. 3. They are obtained from Eq. (5) for the E_0 and $E_0+\Delta_0$ gap contribution, from Eq. (17) for the E_1 gap one, and from Eq. (22) for the E_2 gap one. As indicated in the figure, the E_1 and E_2 gap contributions exhibit the strongest singularity as photon energies approach those of the E_1 and E_2

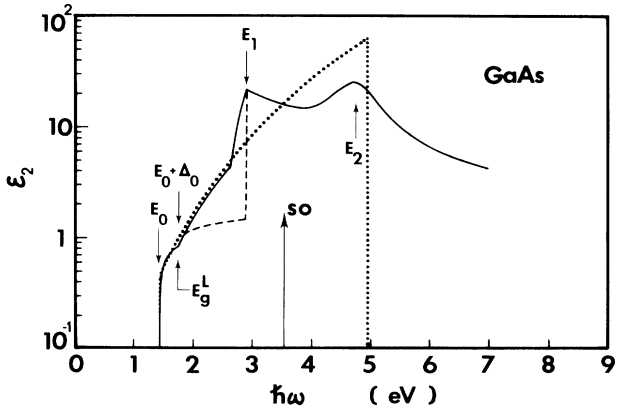

FIG. 2. Representations of the ϵ_2 spectrum of GaAs. The solid line is obtained from the sum of Eqs. (3), (13), (21), and (24). The dashed line is taken by the sum of Eqs. (3), (16), and (21). The dotted line represents the Afromowitz's model [Eq. (24)]. Delta function (so) represents a single-effective-oscillator model (Ref. 16).

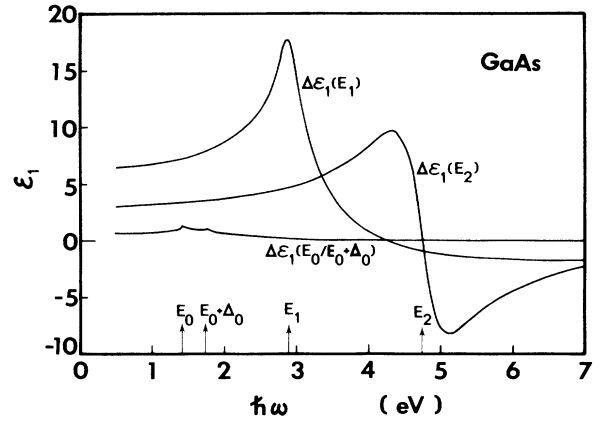

FIG. 3. Individual contribution to ϵ_1 of the E_0, $E_0+\Delta_0$, E_1, and E_2 gaps for GaAs.

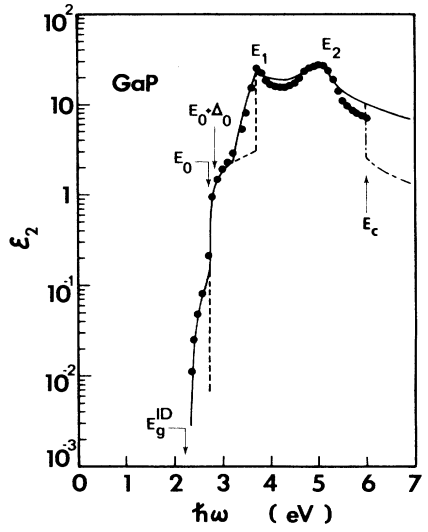

FIG. 4. ϵ_2 spectrum of GaP. The experimental data (solid circles) are taken from Ref. 2. The solid line is obtained from the sum of Eqs. (3), (13), (21), and (24). The dashed line is taken by the sum of Eqs. (3), (16), and (21). The high-energy cutoff correction is represented by the dash-dotted line.

edges. The E_0 and $E_0+\Delta_0$ gap contribution becomes appreciable only in the photon-energy region close to these edges.

The model given above can be used to fit the experimental dispersion of ϵ_1 and ϵ_2 over most of the spectral range (0—6.0 eV). The parameters, such as A, B_1, and Γ, can be commonly used as adjustable constants for calculations of both ϵ_1 and ϵ_2. The experimental data of ϵ_1 in the transparent region are, however, usually somewhat larger than our model [ϵ_1 equal to the sum of Eqs. (5), (17), and (22)]. In order to improve a fit, therefore, we shall consider an additional term, $\epsilon_{1\infty}$, to ϵ_1. This term is assumed to be constant and may arise from the indirect-gap and other higher-gap transitions (E_0', $E_0'+\Delta_0'$, E_1', $E_1'+\Delta_1'$, etc.).

III. ANALYSIS AND DISCUSSION

A. Gallium phosphide

The GaP crystal is known to be a more suitable material to study some of the indirect-gap optical process, since it has three indirect gaps, $\Gamma_8^v \rightarrow X_6^c$ near 2.26 eV, $\Gamma_8^v \rightarrow X_6^c$ near 2.48 eV, and $\Gamma_8^v \rightarrow L_6^c$ near 2.63 eV, as well as the lowest-direct gap E_0, $\Gamma_8^v \rightarrow \Gamma_6^c$ near 2.74 eV. In GaP, the E_1 transitions are known to occur near 3.7 eV. The spin-orbit splitting energy Δ_1 in this material is rather small (<0.1 eV) and can be neglected here. The structure that appeared in the region $\simeq 5.0$ eV is labeled to be E_2.

Figure 4 shows the fit with our model to the experimental ϵ_2 spectrum of GaP. The experimental data are taken from Ref. 2. The solid line is obtained from the sum of Eqs. (3), (13), (21), and (24). The dashed line is the result of the sum of Eqs. (3), (16), and (21). The parameters of the fits are listed in Table I. As clearly seen in the figure, the fit in the fundamental absorption edge region becomes quite satisfactory when the indirect-gap contribution [Eq. (24)] is taken into account. As discussed in Sec. II, we are able to fit the E_1 critical-point structure with either 2D [Eq. (16)] or 3D model [Eq. (13)]. The 3D model well explains the experimental lower-energy shoulder of this structure. The structure in the 6.0-eV region of our model (dash-dotted line) is the result of the cutoff-energy modification [Eq. (18)].

A comparison of our ϵ_1 model to the experimental data of GaP is shown in Fig. 5. The data are taken below 1.5 eV from Ref. 18 and those at higher energies taken from Ref. 2. The solid line is obtained from the sum of Eqs. (5), (17), (22), and $\epsilon_{1\infty}$. The result of the E_c (cutoff) modi-

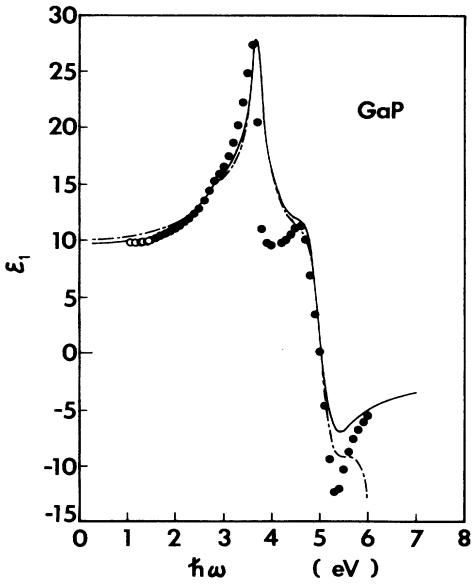

FIG. 5. ϵ_1 spectrum of GaP. The solid and open circles are taken from Refs. 2 and 18, respectively. The solid line is obtained from the sum of Eqs. (5), (17), (22), and $\epsilon_{1\infty}$ ($=0.1$). The high-energy cutoff correction is represented by the dash-dotted line.

fication [i.e., the sum of Eqs. (5), (19), (22), and $\epsilon_{1\infty}$] is also shown in the figure by the dash-dotted line. It is apparent from the figure that the E_c modification provides no notable change in the ϵ_1 spectrum below ~ 5.0 eV. However, to obtain the best fit we must take into account different values of the background contribution $\epsilon_{1\infty}$ in the calculations between the models with and without the E_c modification. Values of this constant are, respectively, 2.1 and 0.1 with and without the E_c modification. A large value of $\epsilon_{1\infty}$ with the E_c modification is required to compensate the cutoff-lossed strength in the ϵ_2 spectrum at above E_c (see Fig. 4).

The E_c modification gives a significant feature in the ϵ_1 spectrum near the cutoff-energy region, i.e., the calculated ϵ_1 spectrum shows a divergence as photon energies approach E_c and becomes nonphysical above this energy. In view of this, we believe that the model of no E_c correction (solid line) provides an ϵ_1 spectrum in much better agreement with the experimental data. A model somewhat similar to those of Eqs. (18) and (19) has also been used in Ref. 9 to investigate the refractive-index dispersion of GaP. However, their analysis is limited in the energy range 1.5—3.5 eV. No attention has, therefore, been paid to structures in the E_1, E_2, and E_c regions.

B. Gallium arsenide

The GaAs crystal is a direct-band-gap semiconductor. The lowest-direct gap E_0 is 1.42 eV at room temperature. The E_1, $E_1+\Delta_1$, and E_2 transitions occur at 2.90, 3.13, and 4.75 eV, respectively. The indirect gaps E_g^L and E_g^X are, respectively, 1.73 and 1.91 eV at room temperature. These indirect transitions may, thus, take part at above the onset of the direct-gap transitions which occurs at 1.42 eV (E_0 gap energy). This is in contrast with the case for GaP in which the indirect transitions occur before the onset of the direct-gap ones.

A comparison of our ϵ_2 model to the experimental data of GaAs is shown in Fig. 6. The experimental data are taken below 1.5 eV from Ref. 18 and above this energy taken from Ref. 2. The solid line is obtained from the sum of Eqs. (3), (13), (21), and (24). The dashed line represents the fit without taking into account the indirect-gap contribution [Eq. (24)] and assuming that the E_1 critical point is to be 2D minimum [Eq. (16)]. The E_1 transitions can contain sufficient strength to represent both E_1 and $E_1+\Delta_1$. Because of this fact, we neglected the $E_1+\Delta_1$ gap contribution [Eq. (14)] and that in Eq. (16) in the calculations. An excellent agreement between our model (solid line) and the experimental data is seen in the figure over the entire spectral range.

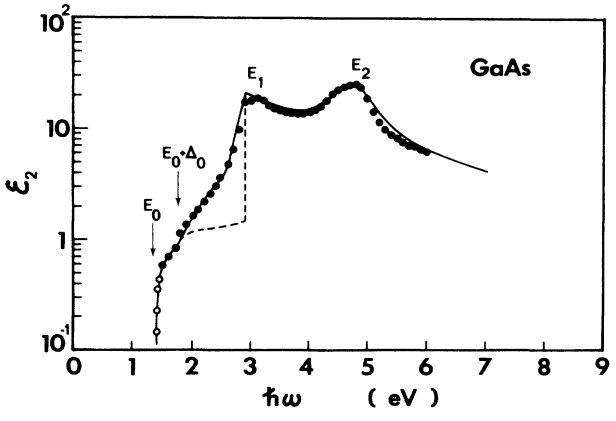

FIG. 6. ϵ_2 spectrum of GaAs. The solid and open circles are taken from Refs. 2 and 18, respectively. The solid line is obtained from the sum of Eqs. (3), (13), (21), and (24). The dashed line is taken by the sum of Eqs. (3), (16), and (21).

The fit with our ϵ_1 model to the experimental data of GaAs is shown in Fig. 7. The data are taken below 1.5 eV from Ref. 18 and above this energy from Ref. 2. The solid line is obtained from the sum of Eqs. (5), (17), (22), and $\epsilon_{1\infty}$ ($=1.2$; see Table I). A rather good agreement between our calculation and the experimental data can be seen in the figure especially in the region below 2.9 eV (E_1 gap). The experimental value of ϵ_1 at the E_1 peak is 23.6.[2] As discussed in Sec. II, the smaller the broadening parameter (Γ) gives the larger the E_1 peak value. The calculation with $\Gamma=0.1$ eV agrees well with this value. Our model of Eq. (22) also well interprets the peculiar line shape of the E_2 structure.

C. Gallium antimonide

Like GaAs, GaSb is a direct-band-gap semiconductor, but GaSb has an indirect gap E_g^L (0.76 eV) very close to the lowest direct gap E_0 (0.72 eV). The E_1 and $E_1+\Delta_1$ gaps are, respectively, 2.05 and 2.50 eV. The spin-orbit splitting energy Δ_1, thus, seems to be considerably larger as compared with those of GaAs and GaP. The E_2 transitions occur in GaSb at ~ 4.0 eV.

A comparison of our ϵ_2 model to the experimental data of GaSb is shown in Fig. 8. The data are taken below 1.0

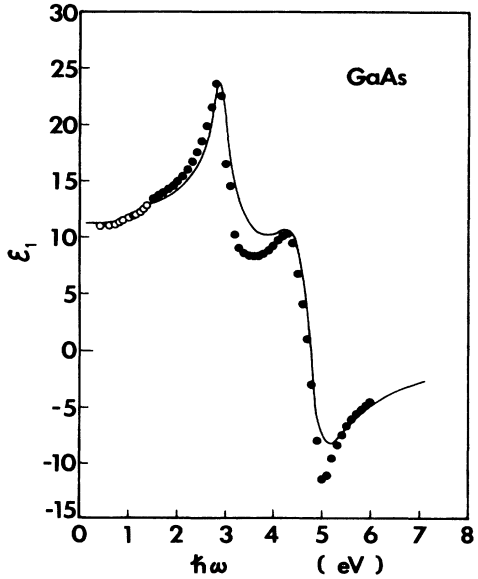

FIG. 7. ϵ_1 spectrum of GaAs. The solid and open circles are taken from Refs. 2 and 18, respectively. The solid line is taken by the sum of Eqs. (5), (17), (22), and $\epsilon_{1\infty}$ ($=1.2$).

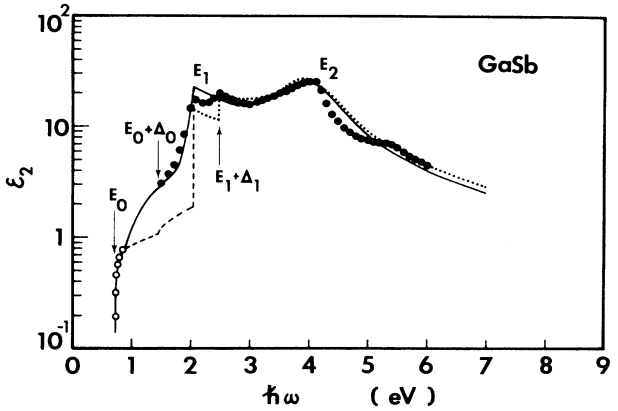

FIG. 8. ϵ_2 spectrum of GaSb. The solid and open circles are taken from Refs. 2 and 18, respectively. The solid line is obtained from the sum of Eqs. (3), (13), (21), and (23). The dashed line is taken by the sum of Eqs. (3), (16), and (21). The dotted line represents the fit with Eq. (16) with taking into account both the E_1 and $E_1+\Delta_1$ gap contributions.

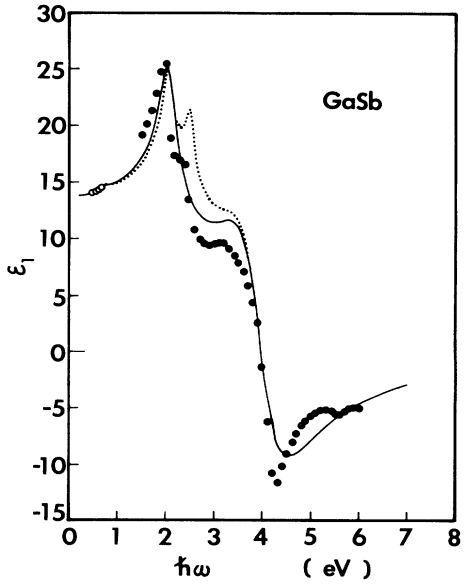

FIG. 9. ϵ_1 spectrum of GaSb. The solid and open circles are taken from Refs. 2 and 18, respectively. The dotted and solid lines are obtained from the sum of Eqs. (5), (17), (22), and $\epsilon_{1\infty}$ (=1.0) with and without taking into account the $E_1+\Delta_1$ gap contributions, respectively.

eV from Ref. 18 and those in the 1.5—6.0-eV range taken from Ref. 2. These data reveal the presence of a weak structure in the 5—6-eV region which was not clearly found in the spectra of GaP and GaAs. This new structure may be due to the E_1' transitions taking place from the top valence band (Λ_3^v) to the second-lowest conduction band (Λ_3^c) near the L point.[5] We do not consider this structure in the analysis of the ϵ_2 spectrum. As discussed in Sec. III, however, the term $\epsilon_{1\infty}$ is introduced to take account of such higher-energy transitions in the analysis of the ϵ_1 spectrum. The solid line represents the result of the sum of Eqs. (3), (13), (21), and (24). The dashed line corresponds to the sum of Eqs. (3), (16), and (21). The $E_1+\Delta_1$ gap contribution is not taken into account in these calculations. As seen in the figure, the indirect gap [Eq. (24)] and 3D saddle-point term [Eq. (13)] well interpret the 1.5—2.0-eV region of the ϵ_2 spectrum.

The strength of the E_1 and $E_1+\Delta_1$ structures of zinc-blende materials can be easily estimated with the simple expression:[3–5]

$$B_1=44\frac{(E_1+\Delta_1/3)}{a_0E_1^2}\ , \tag{27a}$$

$$B_2=44\frac{(E_1+2\Delta_1/3)}{a_0(E_1+\Delta_1)^2}\ , \tag{27b}$$

where a_0 is the lattice constant in Å and E_1, Δ_1 in eV. This expression predicts $B_1=3.78$ and $B_2=2.71$, with a ratio $B_1/B_2=1.39$ and a sum $B_1+B_2=6.49$. The present analysis provides the sum B_1+B_2 equals 6.68. The agreement is extremely good in view of the crudeness of the theory used. The dotted line in Fig. 8 is calculated by introducing the strength parameters of $B_1=3.89$ and $B_2=2.79$ (keeping $B_1/B_2=1.39$ but $B_1+B_2=6.68$) into Eq. (16).

In Fig. 9, we show the fit with our ϵ_1 model to the experimental data of GaAs. The data are taken below 1.0 eV from Ref. 18 and those in the 1.5—6.0-eV range from Ref. 2. The theoretical curves are obtained from the sum of Eqs. (5), (17), (22), and $\epsilon_{1\infty}$ (=1.0). The solid and dotted lines, respectively, represent the fits with the strength parameters of $B_1=6.68$, $B_2=0$ (E_1), and $B_1=3.89$, $B_2=2.79$ ($E_1/E_1+\Delta_1$). As seen in the figure, we obtain a better fit with the solid line rather than with the dotted one. This seems unessential: if one properly chooses the strengths of B_1 and B_2, the difference may actually be lost or a better fit may be achieved. If we try to do this fitting, we obtain a significantly larger strength ratio B_1/B_2, as compared with the ratio obtained from Eq. (27). As in the cases of GaP and GaAs, our model well explains the ϵ_1 spectrum of GaSb especially in the transparent region.

D. Indium phosphide

The interband transition energies of InP are 1.35 eV (E_0), 1.45 eV ($E_0+\Delta_0$), 3.10 eV (E_1), 3.25 eV ($E_1+\Delta_1$), and 4.7 eV (E_2). Like GaP and GaAs, InP has a small value of Δ_1 ($\sim$0.15 eV) and can be neglected here. The lowest indirect gaps E_g^L and E_g^X are, respectively, 2.05 and 2.21 eV.

A comparison of our ϵ_2 model to the experimental data of InP is shown in Fig. 10. The solid line is taken by the sum of Eqs. (3), (13), (21), and (24), and the dashed line is taken by the sum of Eqs. (3), (16), and (21). As seen in the figure, our model (solid line) shows an excellent agreement with the experimental data[2,18] over a wide range of the photon energies.

The fit with our ϵ_1 model to the experimental data of InP (Refs. 2 and 18) is shown in Fig. 11. The theoretical

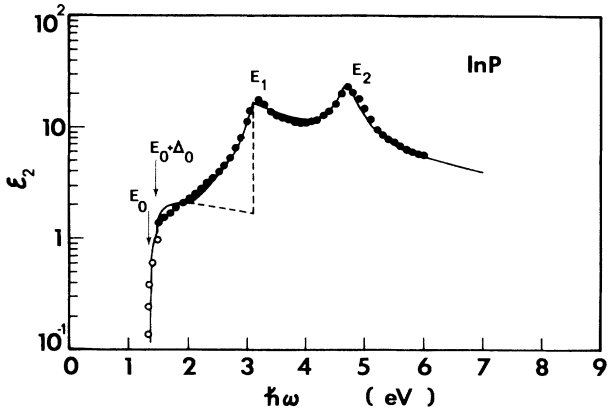

FIG. 10. ϵ_2 spectrum of InP. The solid and open circles are taken from Refs. 2 and 18, respectively. The solid line is taken by the sum of Eqs. (3), (13), (21), and (24), and the dashed line corresponds to the sum of Eqs. (3), (16), and (21).

curve is obtained by the sum of Eqs. (5), (17), (22), and $\epsilon_{1\infty}$ (=1.6). The broadening parameter Γ considered here is 0.1 eV. We see from the figure that in the transparent region ($\hbar\omega \leq 1.35$ eV) the theoretical model gives a good agreement with the experimental data. However, the fit in the E_1 and E_2 regions is poorer than that in the transparent region, although the model well explains the experimental shape of these structures. As already seen in Figs. 5, 7, and 9 and shall also see later (Figs. 13 and 15), this is a general trend holding for fits of our model with the experimental data of all materials studied here. We could not successfully explain the reason for this disagreement at present. A possibility may be that it is due to the effects of excitonic interaction at the E_1 ($E_1+\Delta_1$) and E_2 gaps. Hanke and Sham[19] have shown theoretically that such excitonic effects can modify the optical constants and give rise to shifts of CP structures.

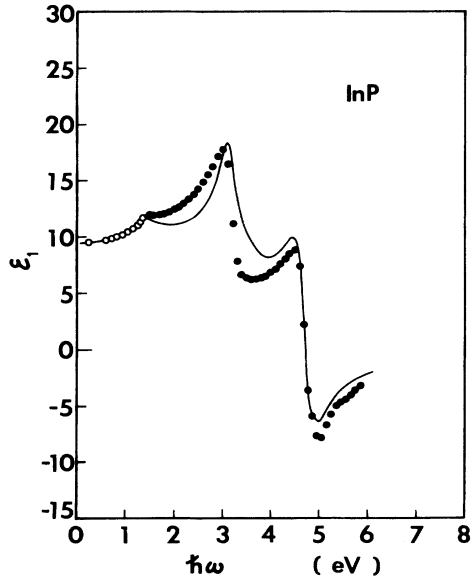

FIG. 11. ϵ_1 spectrum of InP. The solid and open circles are taken from Refs. 2 and 18, respectively. The solid line is obtained from the sum of Eqs. (5), (17), (22), and $\epsilon_{1\infty}$ (=1.6).

E. Indium arsenide

The lowest direct-gap energies E_0 and $E_0+\Delta_0$ of InAs are, respectively, 0.36 and 0.76 eV at room temperature. The higher interband energies E_1, $E_1+\Delta_1$, and E_2 are, respectively, 2.5, 2.78, and 4.45 eV. The lowest indirect-gap energies of this material are $E_g^L=1.07$ eV and $E_g^X=1.37$ eV. The spin-orbit splitting energies Δ_0 and Δ_1 are, respectively, 0.40 and 0.28 eV; these values are nearly equal to E_0.

Figure 12 shows a comparison of our ϵ_2 model with the experimental data of InAs. The solid line is obtained from the sum of Eqs. (3), (13), (21), and (24). The dashed line is obtained from the sum of Eqs. (3), (16), and (21). The $E_1+\Delta_1$ gap contribution is neglected in these calculations. The experimental data are taken below 1.0 eV from Ref. 18 and above 1.5 eV from Ref. 2. The calculated curves reveal considerable structure in the region below E_1 which are difficult to see in Figs. 4, 6, 8, and 10. These arise from the E_0, $E_0+\Delta_0$, and E_g^{ID} gap transitions. Unfortunately, however, the fit with the experimental data is not so good in this energy region. The same situation also holds in the case of InSb (see Fig. 14). This large discrepancy seems to be due to improper assumption of the E_0 and $E_0+\Delta_0$ gaps used in the model [i.e., the parabolic-band assumption; see Eq. (3)]. The nonparabolic characteristic of the band is manifest through a change in apparent effective mass with increase in carrier population.[20] This is prominent in InAs and InSb. A more rigid model should, therefore, be required to improve the fit in such a spectral region for these materials. As in the cases of GaAs and InP, on the other hand, the present model well explains the spectral dependence of the E_1 and E_2 structures.

We show in Fig. 13 the fit of our ϵ_1 model to the experimental data of InAs. The data are taken from Ref. 2 (solid circles) and from Ref. 18 (open circles). The solid

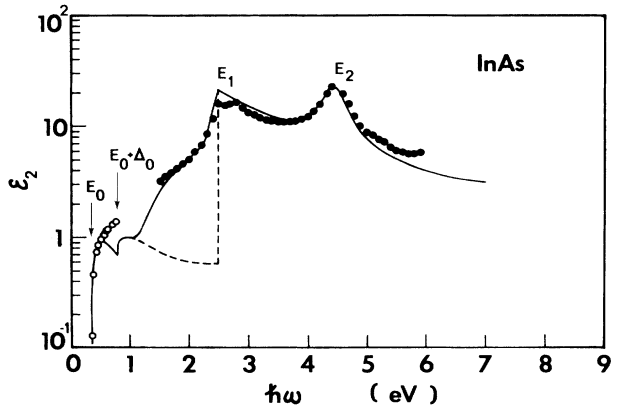

FIG. 12. ϵ_2 spectrum of InAs. The solid and open circles are taken from Refs. 2 and 18, respectively. The solid line is obtained from the sum of Eqs. (3), (13), (21), and (24). The dashed line is taken by the sum of Eqs. (3), (16), and (21).

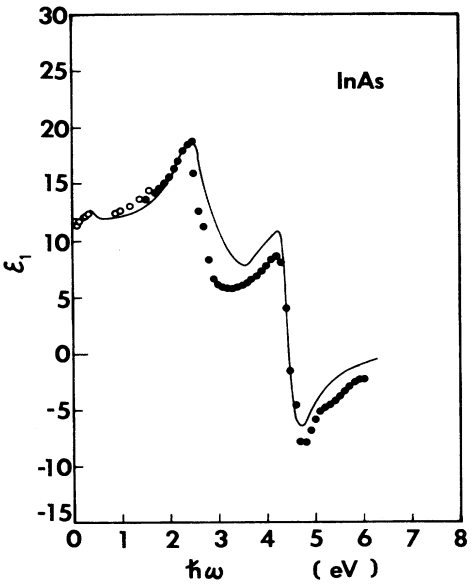

FIG. 13. ϵ_1 spectrum of InAs. The solid and open circles are taken from Refs. 2 and 18, respectively. The solid line is taken by the sum of Eqs. (5), (17), (22), and $\epsilon_{1\infty}$ (=2.8).

line is taken from the sum of Eqs. (5), (17), (22), and $\epsilon_{1\infty}$ (=2.8). General features obtained from this fit are essentially the same as those discussed above.

F. Indium antimonide

InSb has the interband gaps of $E_0=0.18$ eV, $E_0+\Delta_0=0.99$ eV, $E_1=1.8$ eV, $E_1+\Delta_1=2.3$ eV, and $E_2=3.9$ eV. As in the case of InAs, the spin-orbit splitting energies of this material are relatively large ($\Delta_0=0.81$ eV and $\Delta_1=0.50$ eV). This material has also the lowest-indirect gaps of $E_g^L=0.93$ eV and $E_g^X=1.63$ eV.

In Fig. 14, we compare the ϵ_2 spectrum of our model with the experimental data of InSb. The solid line is taken from the sum of Eqs. (3), (13), (21), and (24). The dashed line is obtained from the sum of Eqs. (3), (16), and (21). The experimental data are taken from Ref. 2 (solid circles) and from Ref. 18 (open circles). We recognize in Fig. 14 a considerable deviation of our model (solid line) from the experimental data in the E_0 and $E_0+\Delta_0$ region, i.e., the calculated values of ϵ_2 are too large in this region. As in the case of InAs, this deviation is probably due to the nonparabolic nature of the conduction band at Γ point (E_0 and $E_0+\Delta_0$ gaps). The experimental data reveal the weak E_1' structure in the 5—6-eV region. Logothetidis *et al.*[5] have studied second-derivative features of this structure with a mixture of a 2D maximum and a saddle point.

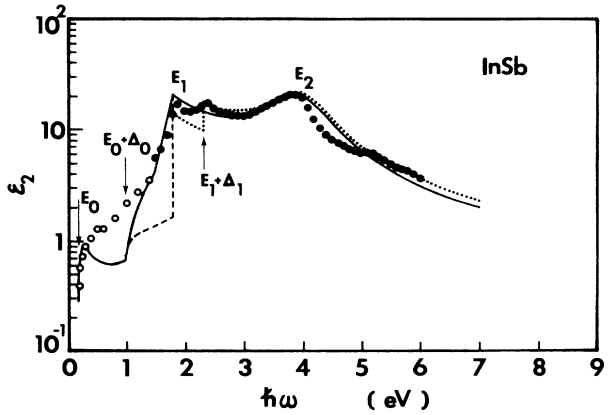

FIG. 14. ϵ_2 spectrum of InSb. The solid and open circles are taken from Refs. 2 and 18, respectively. The solid line is taken by the sum of Eqs. (3), (13), (21), and (24), and the dashed line corresponds to the sum of Eqs. (3), (16), and (21). The dotted line represents the fit with Eq. (16) with taking into account the E_1 and $E_1+\Delta_1$ gap contributions.

The strengths of the E_1 and $E_1+\Delta_1$ structures estimated with Eq. (27) are $B_1=4.12$ and $B_2=2.74$. Our fit provides the sum B_1+B_2 equals 6.37 which compares well with the calculated value ($B_1+B_2=6.86$). The dotted line in Fig. 14 is obtained by introducing strength parameters of $B_1=3.83$ and $B_2=2.54$ (keeping $B_1/B_2=1.50$ [i.e., the ratio of Eq. (27)] and $B_1+B_2=6.37$) into Eq. (16).

We show in Fig. 15 the fit with our ϵ_1 model to the experimental data of InSb. The data are taken from Ref. 2 (solid circles) and from Ref. 18 (open circles). The theoretical curves are obtained from the sum of Eqs. (5), (17), (22), and $\epsilon_{1\infty}$ (=3.1). The solid and dashed lines, respectively, represent the fits with the strength parameters of $B_1=6.37$, $B_2=0$ (E_1), and $B_1=3.83$, $B_2=2.54$ ($E_1/E_1+\Delta_1$). As in the case of GaSb, we see a better fit with the solid line than with the dotted one.

Finally, we note in Table I that A, which represents the strength of the E_0 and $E+\Delta_0$ gaps, is smaller in material with smaller E_0 gap. This is evident from Eq. (4). (Note

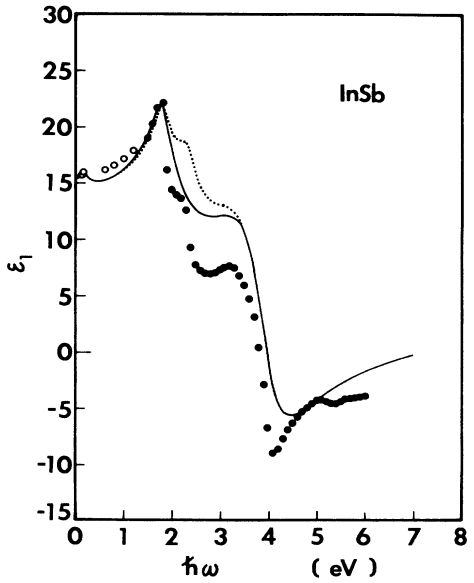

FIG. 15. ϵ_1 spectrum of InSb. The solid and open circles are taken from Refs. 2 and 18, respectively. The dotted and solid lines are obtained from the sum of Eqs. (5), (17), (22), and $\epsilon_{1\infty}$ (=3.1) with and without taking into account the $E_1+\Delta_1$ gap contribution, respectively.

that the smaller E_0 gap material has a smaller m^* value.[21]) The same conclusion has already been reached by us from the analysis of the refractive-index data with the theoretical prediction based on a simplified model of the interband transitions.[14] The strength parameter B in Table I does not vary so widely from material to material. The parameters, Γ, C, γ, D, and $\epsilon_{1\infty}$, on the other hand, vary widely in the materials. No exact quantitative theories, unfortunately, enable us to discuss in detail the justification of these values at present. However, we note that the present model well explains the experimental ϵ_1 and ϵ_2 spectra over the entire range of energies. By performing simple calculations, we can also properly obtain the optical constants, such as the refractive indices and the absorption coefficients, from this model. It is well known that these constants are important for a variety of optoelectronic device applications.

IV. CONCLUSION

We have developed a method for calculation of the real (ϵ_1) and imaginary part (ϵ_2) of the dielectric function of semiconductors at energies below and above the lowest-band gap. The model is based on the Kramers-Kronig transformation and takes into account the effects of interband transitions at the E_0, $E_0+\Delta_0$, E_1, $E_1+\Delta_1$, and E_2 critical points. Line-shape analysis of ϵ_1 and ϵ_2 spectra yields information about the strength and broadening parameters of the critical points. Our model shows a reasonable agreement with the experimental data of both the ϵ_1 and ϵ_2 spectra (GaP, GaAs, GaSb, InP, InAs, and InSb) over the entire range of energies. By performing simple calculations, we can properly obtain the optical constants, such as the refractive indices and the absorption coefficients, which form an important part in the design and analysis of optoelectronic devices. Since the expressions obtained here are purely functions of the fundamental electronic-band parameters, the present model can also be applicable to the analysis of some perturbation-induced effects of the optical constants (e.g., the pressure and temperature dependence of the refractive index, the piezobirefringence, and the light-scattering spectra).

ACKNOWLEDGMENT

The author wishes to thank Dr. M. Fujimoto, Dr. T. Ikegami, Dr. K. Hirata, and Dr. T. Ishibashi for their encouragement.

[1]J. Friedel, G. Harbeke, F. Abeles, B. O. Seraphin, J. Tauc, V. M. Granovich, J. G. Mavroides, M. Balkanski, H. Pick, W. E. Spicer, J. Ducuing, and C. Flytzanis, in *Optical Properties of Solids,* edited by F. Abelés (North-Holland, Amsterdam, 1972).

[2]D. E. Aspnes and A. A. Studna, Phys. Rev. B **27**, 985 (1983).

[3]L. Viña, S. Logothetidis, and M. Cardona, Phys. Rev. B **30**, 1979 (1984).

[4]L. Viña, H. Höchst, and M. Cardona, Phys. Rev. B **31**, 958 (1985).

[5]S. Logothetidis, L. Viña, and M. Cardona, Phys. Rev. B **31**, 947 (1985).

[6]M. Erman, J. P. Andre, and J. LeBris, J. Appl. Phys. **59**, 2019 (1986).

[7]D. E. Aspnes, S. M. Kelso, R. A. Logan, and R. Bhat, J. Appl. Phys. **60**, 754 (1986).

[8]S. Logothetidis, M. Cardona, P. Lautenschlager, and M. Garriga, Phys. Rev. B **34**, 2458 (1986).

[9]K. Strössner, S. Ves, and M. Cardona, Phys. Rev. B **32**, 6614 (1985).

[10]S. Adachi and C. Hamaguchi, Phys. Rev. B **21**, 1701 (1980).

[11]S. Adachi and C. Hamaguchi, Phys. Rev. B **19**, 938 (1979).

[12]M. Cardona, in *Light Scattering in Solids II,* edited by M. Cardona and G. Guntherodt (Springer-Verlag, New York, 1982), p. 119.

[13]C. W. Higginbotham, M. Cardona, and F. H. Pollak, Phys. Rev. **184**, 821 (1969).

[14]S. Adachi, J. Appl. Phys. **53**, 5863 (1982).

[15]See, for example, Ref. 5.

[16]S. H. Wemple and M. DiDomenico, Jr., Phys. Rev. B **3**, 1338 (1971).

[17]M. A. Afromowitz, Solid State Commun. **15**, 59 (1974).

[18]B. O. Seraphin and H. E. Bennett, in *Semiconductors and Semimetals,* edited by R. K. Willardson and A. C. Beer (Academic, New York, 1967), Vol. 3, p. 499.

[19]W. Hanke and L. J. Sham, Phys. Rev. B **21**, 4656 (1980).

[20]E. D. Palik and G. B. Wright, in *Semiconductors and Semimetals,* Ref. 18, p. 421.

[21]S. Adachi, J. Appl. Phys. **53**, 8775 (1982).